# RSC Advances

This is an *Accepted Manuscript*, which has been through the Royal Society of Chemistry peer review process and has been accepted for publication.

*Accepted Manuscripts* are published online shortly after acceptance, before technical editing, formatting and proof reading. Using this free service, authors can make their results available to the community, in citable form, before we publish the edited article. This *Accepted Manuscript* will be replaced by the edited, formatted and paginated article as soon as this is available.

You can find more information about *Accepted Manuscripts* in the **Information for Authors**.

ROYAL SOCIETY OF CHEMISTRY

www.rsc.org/advances

# RSC Advances

## ARTICLE

# Homogeneous vertical ZnO nanorod arrays with high conductivity on an *in situ* Gd nanolayer†

*Tahani H Flemban, S. Venkatesh, S. Assa Aravindh, Iman S Roqan\**

We demonstrate a novel, one-step, catalyst-free method for the production of size-controlled vertical highly conductive ZnO NR arrays with highly desirable characteristics by pulsed laser deposition using a Gd-doped ZnO target. Our study shows that an *in situ* transparent and conductive Gd nanolayer (with a uniform thickness of ~1 nm) at the interface between a lattice-matched (11-20) *a*-sapphire substrate and ZnO is formed during the deposition. This nanolayer significantly induces relaxation mechanism that controls the dislocation distribution along the growth direction; which consequently improves the formation of homogeneous vertically aligned ZnO NRs. We demonstrate that both the lattice orientation of the substrate and the Gd characteristics are important in enhancing the NR synthesis, and we report precise control of the NR density by changing the oxygen partial pressure. We show that these NRs possess high optical and electrical quality, with a mobility of 177 $cm^2$ $(V.s)^{-1}$, which is comparable to the best-reported mobility of ZnO NRs. Therefore, this new and simple method has significant potential for improving the performance of materials used in a wide range of electronic and optoelectronic applications.

## Introduction

Transparent metal oxide nanostructures are promising materials for several potential applications. In particular, the unique optical, electrical, chemical and ferroelectrical properties and multiple functionalities of ZnO nanorods (NRs)[1-4] have led many researchers to pursue new synthesis methods with the goal of obtaining high-performance nanoscale devices,[3] such as photovoltaic,[4-6] field emitters,[7, 8] solar cells,[9-12] sensors,[13-15] photoelectrochemical water splitting,[16] and nanogenerators.[17-19] However, the fabrication of practical ZnO NR-based devices is hindered as controlling the density, shape, size, and growth direction of well-defined vertical ZnO NRs with high conductivity remains a significant challenge.[2, 3, 20-24] Several methods that employed metal catalyst to grow the NRs are avoided due to lack of transparency and metal contamination, which reduces the material efficiency. Therefore, metal catalyst is not suitable for practical devices, especially optoelectronic applications.[2, 3, 20] Moreover, catalyst-free methods employing interfacial textured layers between the NRs and the substrate were not successful in controlling the desired vertical NR structure.[25-30] In addition, the interfacial layer should be conductive and transparent for use in devices.[26] Consequently, such a layer would be able to,

for example, serve as a common electrode to connect NRs with an external circuit of devices.[31] Therefore, there still no method that are capable of controlling the structure of well-defined, homogeneous transparent metal oxide NRs for high efficiency devices.

In this work, we present a novel method that allows us to overcome the previously mentioned difficulties, using pulsed laser deposition (PLD). In several studies, PLD systems were used to grow NRs by employing special set-ups that required a priori textured layers[25, 26, 28] and/or a customized high-pressure chamber (a few to several hundred Torr).[32-35] However, thus far, none of these PLD methods has been successful.

Our approach enables the production of homogeneous (with respect to height and diameter) arrays of vertical self-assembled hexagonal ZnO NRs grown on transparent substrates using rare earth (RE) dopants. The formation of an *in situ* homogeneous ultra-thin RE nanolayer (with a uniform well-defined thickness) at the interface between a lattice-matched substrate and the ZnO NRs is the key factor characterizing our approach for obtaining control over the NR structures and their electrical properties. We show that the *in situ* RE nanolayer assists in producing well-aligned state-of-the-art conductive ZnO NRs with homogeneous heights and sizes. Our method benefits from the use of RE dopants in the RE:ZnO PLD target. In particular, gadolinium (Gd) dopants do not reduce the optical efficiency of ZnO NRs.[36]

*Physical Sciences and Engineering Division, King Abdullah University of Science and Technology (KAUST), Thuwal 23955-6900, Saudi Arabia. E-mail: iman.roqan@kaust.edu.sa*

## Experimental

### Synthesis of ZnO NRs.
Gd-doped ZnO laser ablation targets were prepared by mixing
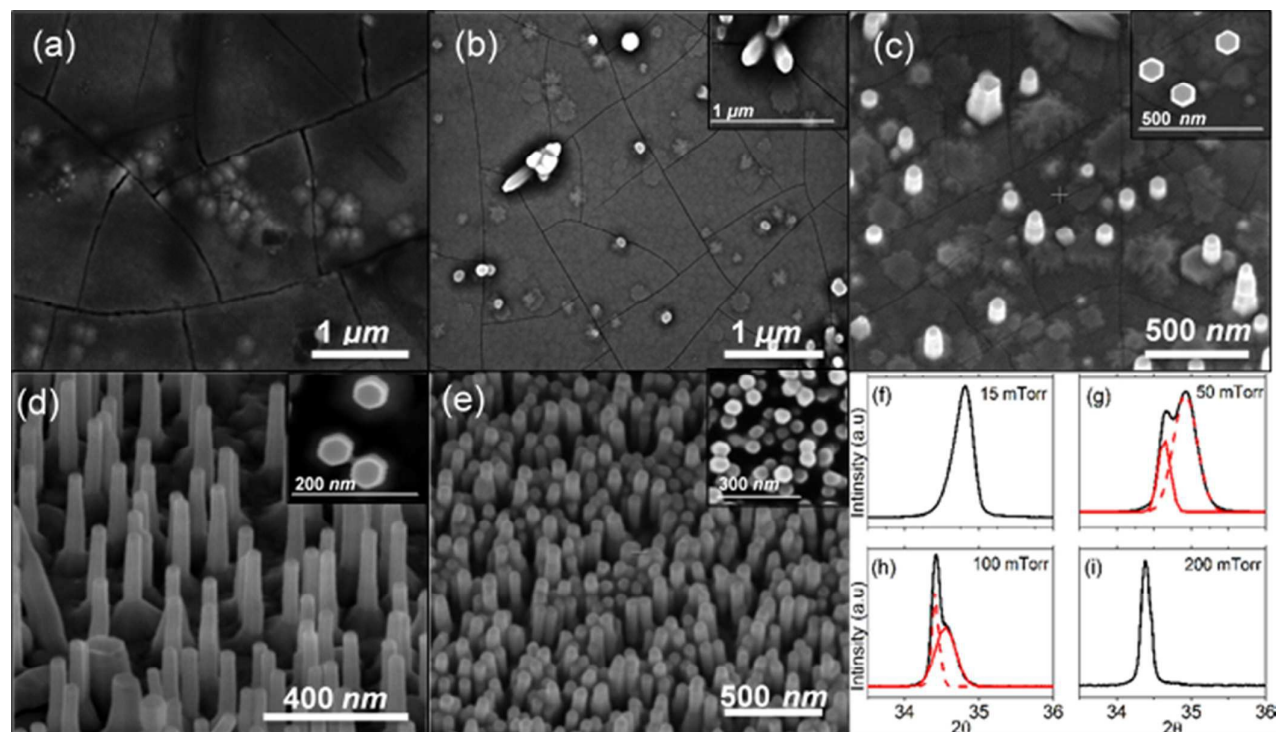
Fig 1. SEM images of Gd-doped ZnO samples grown on $a$-Al$_2$O$_3$ at (a) $P$(O$_2$) = 15 mTorr, (b) 25 mTorr, (c) 50 mTorr, (d) 100 mTorr, and (e) 200 mTorr. The insets of the Figs (b-e) show the top view. XRD patterns of these Gd-doped ZnO samples; the high angle shoulder represents the XRD peak from the film. The dashed and solid red lines indicate Gaussian fits of the peaks for the NRs and the film, respectively.

99.75 wt% pure ZnO (99.999%) powder with 0.25 wt% Gd$_2$O$_3$ (99.99%) powder (Sigma-Aldrich-US). A pellet with a diameter of 2.5 cm was pressed and sintered at ~ 1100 $^o$C for 12 h to produce a dense, 2.3-cm-diameter disc. To grow the ZnO NRs, we used the Gd 0.25 wt%-doped ZnO target. A PLD system (Neocera, Pioneer 240) equipped with a krypton fluoride (KrF) excimer laser (λ = 248 nm) was used to ablate the Gd (0.25 wt%)-doped ZnO target. The substrate was mounted at a large distance (~9 cm) vertically above the target, and the vacuum chamber was pumped to 10$^{-6}$ Torr before target ablation. Next, the growth temperature was set to 650 $^o$C. The ZnO NRs were grown on lattice-matched (11-20) $a$-Al$_2$O$_3$ by focusing the beam on the Gd-doped ZnO target surface with a beam fluency of 5 ± 0.5 J/cm$^2$. The deposition consisted of 30,000 laser pulses delivered at a frequency of 10 Hz. To control the NR density, $P$(O$_2$) was varied in the range of 15-200 mTorr for all samples. For comparison, Gd-doped ZnO was deposited on (0001) $c$-Al$_2$O$_3$, while undoped ZnO was deposited on both $a$-Al$_2$O$_3$ and $c$-Al$_2$O$_3$ under the same growth conditions.

**Characterizations.** Morphologies and crystallization were characterized by scanning electron microscopy (SEM) (FEI Nova Nano 630), x-ray diffraction (XRD) (Bruker D8 Discover high resolution XRD with CuKα and λ = 1.5406 Å) and high-resolution transmission electron microscopy (Titan-HRTEM). The electrical properties of our samples were investigated using Hall-effect measurements in a physical property measurement system (PPMS EverCool, Quantum design) by adapting the van der Pauw geometry, with B perpendicular to the direction of the current flow. Photoluminescence (PL) measurements were performed using a 325-nm He-Cd laser with a beam power of ~ 8 mW. The samples were mounted in a He closed cycle cryostat system for low-temperature PL measurements (6.5 K). Room temperature (RT) absorption measurements were carried out using UV-VIS Varian Cary 5000 spectrophotometry. Cathodoluminescence (CL) maps and secondary electron (SE) images were taken at RT using an FEI Quanta 250 environmental FEGSEM. The electron beam energy was fixed at 5 keV. An Andor spectrograph with a charge coupled device camera was used to detect the spectra.

## Results and discussion

Fig 1 shows SEM images of samples deposited on $a$-Al$_2$O$_3$ (with a lattice mismatch of 0.08% between (11-20) $a$-Al$_2$O$_3$ and (0001) ZnO)[37] using a Gd-doped ZnO target. Samples prepared at a partial oxygen pressure $P$(O$_2$) = 15 mTorr are characterized by a continuous film (Fig 1a). ZnO NRs begin to emerge as $P$(O$_2$) increases to 25 mTorr (Fig 1b), whereas low-density ZnO NRs are obtained at $P$(O$_2$) = 50 mTorr (Fig 1c). The spacing between these ZnO NRs is well controlled by changing the $P$(O$_2$). Homogeneous, well-defined, ordered vertical hexagonal ZnO NR arrays are achieved at $P$(O$_2$) = 100 mTorr (Fig

1d) and 200 mTorr (Fig 1e), with average densities of ~80 and ~120 NR/$\mu m^2$, respectively. The NR length is relatively homogeneous (approximately 300 nm). The NR crystalline structure was investigated using high-resolution XRD measurements. Samples deposited at $P(O_2)$ = 15 mTorr show strong peaks at $2\theta$ = 34.79° with a full width at half maximum (FWHM) of 0.314°, which corresponds to a (0002) ZnO plane (11-20) $a$-Al$_2$O$_3$ substrate, indicating a single crystal film grown along the c-axis (Fig 1f). We also observed a shift in the (0002) XRD peak of the Gd-doped ZnO film towards higher angles compared to the undoped ZnO film, which was attributed to vacancies accompanying Gd incorporation into the crystal.[38] For samples deposited at $P(O_2)$ = 50 mTorr, this thin film peak overlaps with the NR peak located at a smaller $2\theta$ = 34.63° (Fig 1g). As the NR density increases with $P(O_2)$, the corresponding XRD peak at $2\theta$ = 34.39° becomes dominant, as shown for samples deposited at $P(O_2)$ = 100 and 200 mTorr. The FWHM of the XRD peak of the ZnO NRs is approximately 0.15°, which is comparable to the best value reported for ZnO NRs,[39-41] indicating the high crystallinity of these ZnO NRs grown along the $c$-axis.

To study the effects of substrate mismatch on NR synthesis, we used the same Gd-doped ZnO target to perform deposition at $P(O_2)$ = 100 mTorr on a (0001) $c$-Al$_2$O$_3$ substrate, which has a high lattice mismatch of ~31.8% with (0001) ZnO[37], for the same deposition conditions of the samples presented in Fig 1. For this sample, random (rather than well-defined) ZnO NRs are observed, as shown in Fig 2a. Furthermore, pure ZnO samples were deposited on $a$-Al$_2$O$_3$ and $c$-Al$_2$O$_3$ at $P(O_2)$ = 100 mTorr to study the effect of Gd doping on the formation of the NRs. Pure ZnO deposited on $a$-Al$_2$O$_3$ is characterized by a low density of nanocrystals (Fig 2b), whereas the sample grown on $c$-Al$_2$O$_3$ shows a continuous film with a rough granular surface morphology (Fig 2c). Therefore, we conclude that, under particular deposition conditions, both the Gd dopant and the Al$_2$O$_3$ substrate orientation are crucial for the
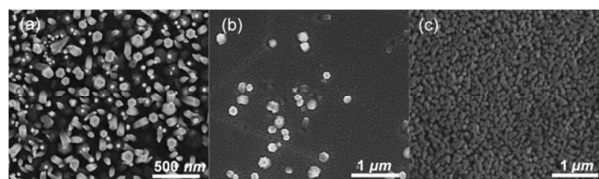


Fig 2. SEM images of (a) Gd-doped ZnO on $c$-Al$_2$O$_3$, (b) undoped ZnO on $a$-Al$_2$O$_3$, and (c) undoped ZnO on $c$-Al$_2$O$_3$. All samples were deposited at $P(O_2)$ = 100 mTorr.

formation of vertical, well-defined, well-ordered ZnO NRs.

We observe that the ZnO NR density increases with increasing $P(O_2)$. This relationship arises from the correlation between the species energy $E$ and the background pressure $P$ —$P(O_2)$ in the present case, which is described by[42]

$$E = E_o \exp(-d/\lambda), \qquad (1)$$

where $E_o$ is the initial energy of the charged species escaping from the target and $d$ is the distance between the target and the substrate (~9 cm). $\lambda$ is the mean free path of the ablated species (the plasma) traveling towards the substrate in the PLD chamber and can be defined as

$$\lambda = kT/\sqrt{2}\pi d_o^2 P, \qquad (2)$$

where $d_o$ is the diameter of the gas molecule, $T$ is the temperature and $k$ is Boltzmann's constant. Therefore, $\lambda$ increases with decreasing $P$, and the kinetic energy of the species on substrate "$E$" decreases exponentially as $P$ increases, which explains the variation in the NR density with changing pressure. Therefore, at higher $P(O_2)$ > 15 mTorr, the ablated species experience a large number of collisions with oxygen molecules, and the condensation of the species on the substrate result in low $E$ that can lead to a Stranski-Krastanov (SK) nucleation and the formation of NRs. At lower $P(O_2)$ (< 15 mTorr), the ions emitted from the target surface with high $E$ after the laser interaction condense on the substrate surface, that can be high enough to form a continuous film.
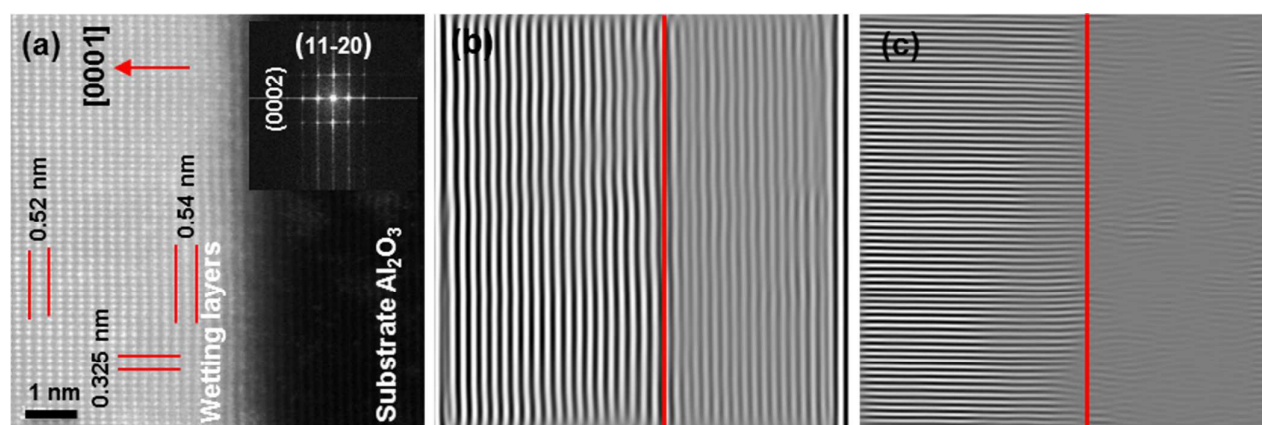


Fig 3. (a) HRTEM image of a vertical cross-section near the interface between substrate and wetting layers. The inset shows the FFT. IFFT (after the masking process by the Digital Micrograph software), (b) from (0002) spots, and (c) from (11-20) spots in the inset of (a) (The red line indicates the interface location).
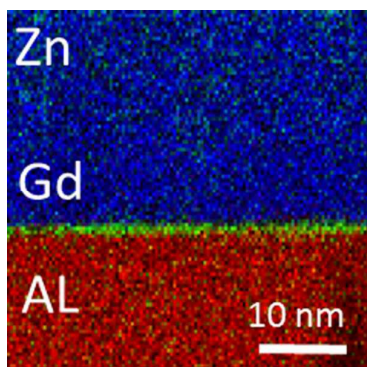
Fig 4. EDS maps of Gd-Lα (green), indicating a uniform interfacial Gd layer between the substrate and the ZnO (The green spots shown in the substrate and films are just noise, as signal to noise ratio is extremely low and EDS technique is not sufficiently sensitive to detect such low composition), Zn-Kα (blue), and Al-Kα (red) near the interface

### Growth mechanism

It is known that structural defects, such as stacking faults, threading dislocations, and grain boundaries, affect the NR growth orientation.[24, 43-45] Therefore, investigating the structural defects near the interface between the substrate and the Gd-doped ZnO wetting layer is essential for a better understanding of the growth mechanism.[44] For this purpose, a cross-section along the *c*-axis of the NRs sample (Fig 1c) was analyzed by HRTEM. We observe that the Gd-doped ZnO wetting layer is a single crystal with [0001] growth direction. Moreover, Fig 3a shows that the value of *c* lattice parameter is greater (0.54 nm) near the interface compared to that away from the interface (0.52 nm, which is comparable to the *c* parameter value of bulk ZnO), indicating that the wetting layer is strained near the substrate and starts to relax homogeneously along *c*-axis as the thickness increases (as shown in the Inverse Fast Fourier Transform (IFFT) (Fig 3b)). However, no strain is observed along the *a*-axis, as we find that the value of *a* parameter (0.325 nm) is similar to that of bulk ZnO, as shown in Fig 3a and 3c. Interestingly, although *c* parameter reaches the ZnO bulk value in a critical thickness, no threading dislocations are observed along *c*- and *a*-axis near the substrate interface.

We investigate chemical compositions near the interface to identify the origin of this uniform strain behavior as the thickness of the wetting layer increases. Energy-dispersive x-ray spectroscopy (EDS) maps of Gd, Zn and Al near the interface are shown in Fig 4, which confirms that our method enables the formation of an *in situ* Gd interfacial nanolayer with a uniform ultra-thin thickness of ~1 nm during deposition. Similarly, electron energy loss spectroscopy (EELS) in different positions near the interface confirms that Gd precipitates near substrate (Fig. S1, ESI,†). Forming Gd nanolayer based on the self –purification of ZnO. When impurity solubility is low, and required high energy to be incorporated into the materials, the impurities The impurities preferentially defuse to the surface or the interface of materials.[46] As Gd concentration increases in the interface, the growth temperature can provide a sufficient energy to Gd atoms in the wetting layer to be diffused near the interface.
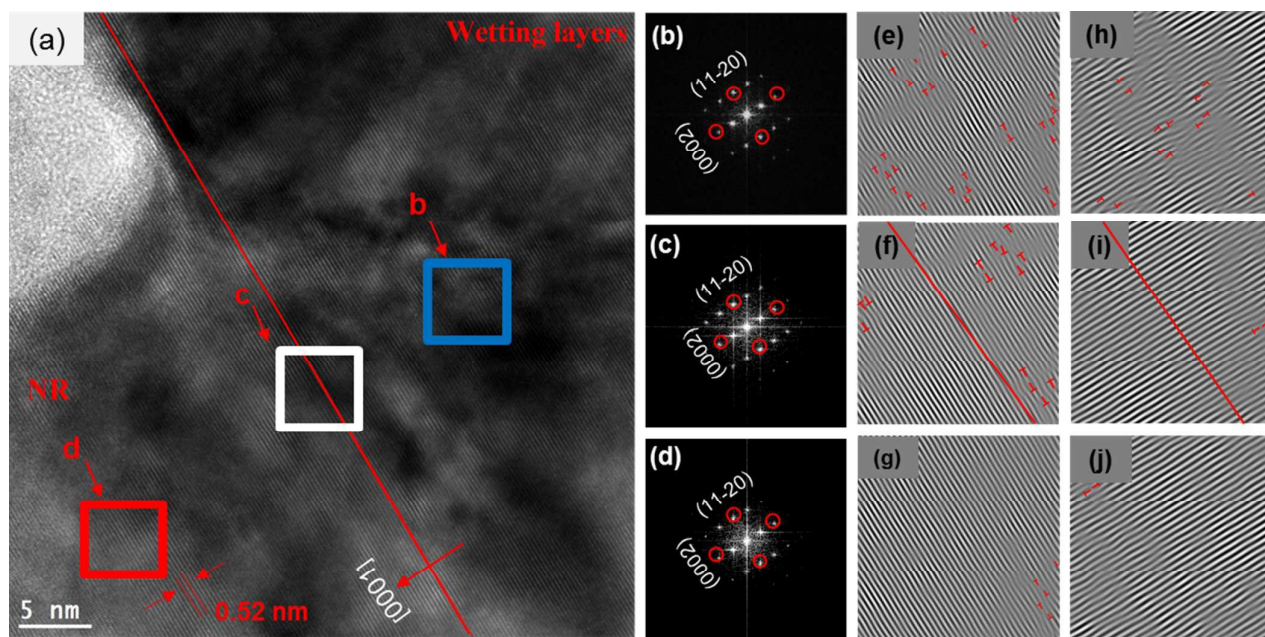


Fig 5. (a) TEM image near the interface between wetting layers and NR. (b) FFT image from the blue-boxed region in (a), and corresponding IFFT from (e) the (0002) spots and (h) the (11-20) spots in (b). (c) FFT image from the white-boxed region in (a), and corresponding IFFT from (f) the (0002) spots and (i) the (11-20) spots in (c). (d) FFT image from the red-boxed region in (a), and corresponding IFFT from (g) the (0002) spots and (j) the (11-20) spots in (d). (The red line indicates the interface location).
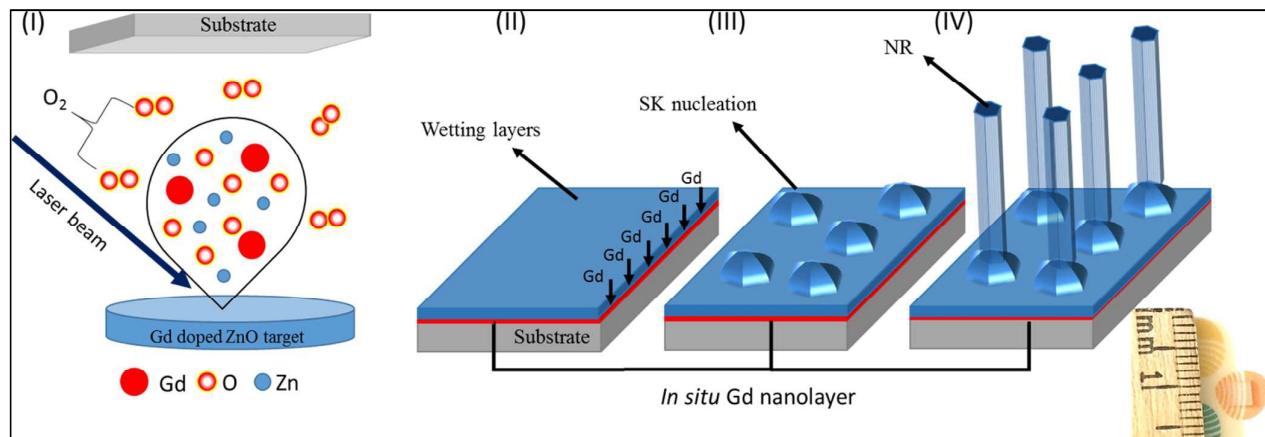
Fig 6. Schematic diagram represents the growth mechanism of NRs. The inset is a photographic image of the sample deposited at $P(O2)$ = 200 mTorr (with the highest density of NRs).

This diffusion of Gd atoms may occur by different surface diffusion mechanisms.[47, 48] In PLD, the atoms falling on a substrate have a kinetic energy $E$ obtained in evaporation or ablation processes, as shown in Eq 1. Then these atoms diffuse on the substrate surface. The probability $p$ of an atom jumping from one lattice site to the other one is given by:[47, 48]

$$p = A exp \left( -E_a/kT \right), \tag{3}$$

where $A$ is the hopping rate, $E_a$ is the surface diffusion energy, and $T$ is the substrate temperature, which is a very important parameter of the PLD method.

We believe that this *in situ* Gd nanolayer acts as a uniform catalyst layer as Gd is metal that assists in forming of Gd-doped ZnO wetting layers with homogenous thickness (Fig. S2, ESI,†) and, therefore, uniform nucleation sites, leading to such ZnO NRs. This explains the absence of NRs in undoped ZnO samples grown on either $a$- or $c$-Al$_2$O$_3$ substrates.

To investigate the effect of this Gd nanolayer on the strain relaxation mechanism as the thickness of the wetting layer increases and in turn formation of the vertical NRs. Therefore, we study the HRTEM near the interface between the wetting layer and the NR (Fig 5a). FFT images (Figs 5b-d) confirm that both the wetting layer and the NR are single crystals with growth along [0001]. Edge dislocations (denoted by the symbol "T" in Figs 5e-j) are observed near the interface between the wetting layer and NR along both $c$- and $a$-axis. We find that the density of dislocations along the $c$-axis (Figs 5e-g) is greater than that along the $a$-axis (Figs 5h-j). Moreover, as the relaxation increases with the wetting layer thickness, the dislocation density near the interface between the NR and the wetting layer increases (Figs 5e and 5h), which can be due to a complete strain relaxation.[49] However, this density decreases in (Figs 5f and 5i) and above the interface (Figs 5g and 5j). Remarkably, Figs 5f and 5i indicate a rapid reduction in the dislocation density in the interface (see the area circled with yellow in Fig. S3, ESI,†) and increases again slightly above the interface in the bottom of the NR. This relaxation mechanism leads to SK nucleation process, which stimulates the growth of homogeneous vertical ZnO NRs with well-defined morphologies. Therefore, at a specific $P(O_2)$, we assume that the formation of a uniform *in situ* Gd nanolayer assists in creating a wetting layer with a homogenous relaxation mechanism to form homogenous ZnO nucleation for vertical orientated NRs.

The nucleation is strongly influenced by the surface energy of the free substrate ($\gamma_s$), the interface between the substrate and the wetting layers; in this case, the Gd nanolayer ($\gamma_i$), and the nucleation facet plane ($\gamma_n$) correspond to the minimum surface energy.[50] In SK case, the surface energy of the substrate exceeds the combination of both surface energy of interfacial wetting layers and nucleations.[50]

$$\gamma_s > \gamma_i + \gamma_n , \tag{4}$$

The same mechanism is employed to explain the absence of ZnO NRs on $c$-Al$_2$O$_3$. More specifically, no vertical and well defined NRs are observed on the sample deposited on the $c$-Al$_2$O$_3$ (Fig 2a) due to a decrease in $\gamma_s$, as the relative surface energies of (11-20) $a$-Al$_2$O$_3$ and (0001) $c$-Al$_2$O$_3$ were estimated to be $\gamma_{(11-20)}$ = 1.12 $\gamma_{(0001)}$.[51] Therefore, the $a$-Al$_2$O$_3$ substrate surface energy and the uniform interfacial Gd nanolayer doping can play a significant role in the growth of high quality vertically aligned hexagonal ZnO NRs.

We can summarize the mechanism of our catalyst-free aligned ZnO NRs, as shown in Fig 6. The laser beam was focused on a ZnO target doped with Gd to evaporate Zn, O, and Gd atoms. In this arrangement, the $P(O_2)$ controls the number of collisions between oxygen molecules and those of the ablated species (Fig6 step-I). Fig 6 step-II shows that the ablated species condense on the above substrate as a wetting layer, forming homogenous *in situ* Gd nanolayer in the interface near the substrate, due to Gd diffusion. The strain of the witting layer above Gd nanolayer increases with thickness. When the strain of the wetting layer exceeds a critical point, SK nucleation will be formed, decreasing the total strain energy (Fig 6 step-III). SK nucleation is a favorable site for NRs growth. Our method demonstrated that homogeneous vertical NRs can be grown along the $c$ direction (step-IV) on a transparent *in situ* Gd layer, without the need for
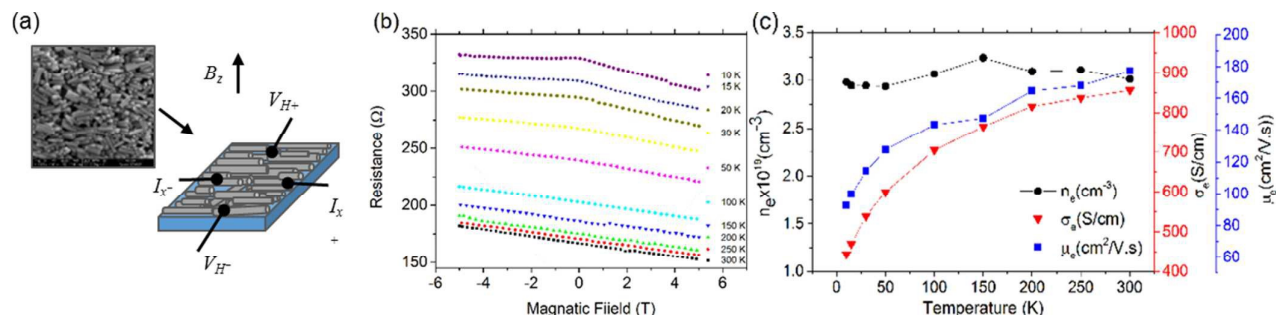
Fig 7. (a) Schematic drawing of the Hall measurement contact for a NR sample grown on $a$-Al$_2$O$_3$ and the corresponding SEM image. (b) Hall measurements at different temperatures and (c) the mobility, carrier concentration and conductivity in the NRs as a function of temperature.

a prefabricated textured or metal catalyst layer.[12, 29] Moreover, the transparency of samples is not affected by Gd *in situ* nanolayer, as shown in the photographic image of the 200 mTorr sample (The inset of Fig 6), indicating its potential use in optoelectronic devices.

In other catalyst-free method that have been previously employed for PLD growth, NRs were produced using customized high gaseous pressure (several Torr) chamber or prefabricated textured layer.[25, 29, 32] High gaseous pressure used during deposition to reduce the kinetic energy of ablated species due to collisions with gas molecules, which leads to the condensation of ablated species and form nanoparticles that act as nucleation sites.[32, 33, 52]

**Enhancement of the electrical properties of the NRs.**

The sample deposited at $P(O_2)$ = 200 mTorr was selected for further study due to its high NR density. This high density allowed us to obtain Ohmic contacts with the NRs after setting them horizontally, as shown in the SEM image (given in the inset of Fig 7a), on the $a$-Al$_2$O$_3$ substrate to provide a more accurate estimation of the conductivity and mobility (the scheme in Fig 7a). Sun *et al.*[53] used the same approach to design a field-effect transistor based on NRs. Therefore, our aim was to measure the overall mobility for applications in various devices. We measured the Hall voltage to estimate the carrier density from the Hall resistance ($R$). Fig 7b shows $R$ as a function of the applied magnetic field ($B$) obtained at different temperatures (T = 10-300 K). $R$ decreases with increasing $B$, indicating n-type conduction.

The electron concentration ($n_e$) is calculated from d$R$/d$B$ by taking into account the NR geometry. Fig 7c shows the temperature dependence of the conductivity ($\sigma_e$), electron mobility ($\mu_e$), and $n_e$. The observed variation of $\sigma_e$ with temperature indicates semiconducting behavior. $n_e$ varies from ~ 1-3 × 10$^{19}$ cm$^{-3}$ with temperature (T). At RT, the $\sigma_e$ and $\mu_e$ values for these NRs are high compared to the previous literature for n-type ZnO NRs,[42, 54, 55] and are estimated to be 855 S/cm and 177 cm$^2$ (V.s)$^{-1}$, respectively. The observed high mobility and conductivity can be due to the high crystalline quality of the NRs and the Gd incorporation. Thus, to confirm the effects of the Gd dopants, we performed density functional theory (DFT) calculations for the electronic structure

of a wurtzite Zn$_{48}$O$_{48}$ NR grown in the [0001] direction with and without Gd doping. To obtain an optimized geometry, the atomic coordinates of the NR were relaxed in both cases. Calculations were performed using the Vienna Ab-initio Simulation Package within the generalized gradient approximation (GGA)[56, 57] and with a plane wave cut-off energy of 400 eV. We employed pseudopotentials based on the projector augmented wave formalism for the spin polarization calculations.[58] A 1×1×8 Monkhorst-Pack k-grid was used to perform the Brillouin zone sampling investigations, using GGA and GGA+$U$ for Gd-doped semiconductor systems yielded very similar results, indicating that the qualitative picture is largely unchanged, and only some minor quantitative differences were detected [59-61]. Hence, we do not expect our results to be significantly altered if GGA+$U$ or SIC-LDA is employed to treat the Gd-doped GaN nanowires.

Figs 8a and 8b show the band structure (BS) of the pristine ZnO NR and Gd-doped ZnO NR, respectively. The BS is estimated along the Gamma to Z direction, which is parallel to the growth direction of the NR. The NR band gap is calculated to be 1.6 eV, which is greater than that obtained for the bulk ZnO using the GGA due to quantum confinement effects. Qualitatively, the GGA allows for a better understanding of the band structure, even though the experimental value of the band gap is an underestimate. The undoped ZnO NR exhibits semiconducting properties and has a direct band gap at the Gamma point, as shown in Fig 8a. A significant shift in the Fermi level into the conduction band can be observed when Gd dopants are introduced, as shown in Fig 8b, which explains the high conductivity and mobility of the NRs (in agreement with our experimental findings). Detailed electronic properties are shown elsewhere.[62] X-ray absorption spectroscopy found that Gd remains Gd$^{3+}$ state; whereas Zn atom remains Zn$^{2+}$ state in Gd doped ZnO samples. Near edge X-ray absorption fine structure spectra at the O K-edge and Gd M5,4-edges indicated that Gd atoms replace Zn sites.[38, 63] Therefore, the incorporation of Gd dopants creates a donor band below the conduction band maximum. Due to the donor band created near the CBM, a shift in the Fermi level occurs, and the material conductivity increases. In addition, we observed a strong spin splitting phenomenon.

ARTICLE
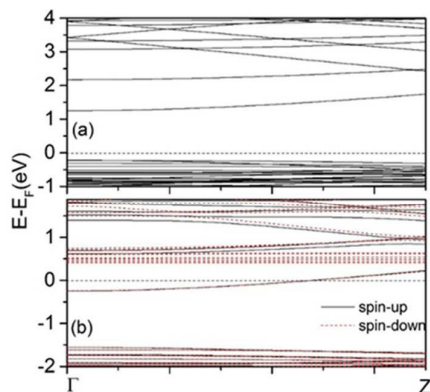


Fig 8. Calculated band structure of (a) undoped ZnO NRs and (b) Gd-doped ZnO NRs. The Fermi energy is set to zero.

**Optical properties of the ZnO NRs.**

Fig 9 shows the low temperature PL (6.5 K) of Gd-ZnO films and NRs prepared at $P(O_2)$ = 15, 25, 50, 100, and 200 mTorr. The ZnO NRs grown at 200 mTorr show strong and sharp UV near-band-edge (NBE) luminescence caused by the neutral donor-bound exciton ($D_oX$) line at 369.16 nm (3.36 eV), with a narrow FWHM of 7.9 meV. The PL band observed at 3.33 eV is due to donor-to-acceptor (DAP) pair transitions.[64] No deep level (DL)-related defects is observed, indicating high optical quality. In particular, the optical efficiency of ZnO is not reduced by Gd incorporation, as the first excitation level of *4f* in $Gd^{3+}$ ion is above the band gap.[36] Therefore, no efficient energy can be transferred from electron-hole recombination in ZnO to *4f* levels, and therefore, no reduction in bandage emission occurs due to energy transfer.[36]

The RT absorption measurements were carried out for ZnO NRs grown at $P(O_2)$ = 200 mTorr (since this sample exhibits PL dominated by NRs emission) as shown in Fig 9b. It can be observed that the ZnO NRs band gap is red shifted (~3.22 eV), compared to bulk ZnO (3.37 eV at RT),[65] may be due to tensile stress. The absorption spectrum exhibits step-like character, indicating high crystal quality. A slight tail shown in absorption spectrum might be due to edge dislocations or inhomogeneous strain in the wetting layers.[66]

CL maps taken in the same area as secondary electron (SE) images are shown in Fig 10 at RT, which allow us to investigate the nanoscale luminescence properties of a single NR.

The CL spectrum can be collected at each point in the map; therefore, the peak fitting allows for an analysis of the spectral parameters, such as the peak energy, width and emission intensity.[67] The RT-CL map reveals that the NBE peak position of NRs has a slight redshift (~3.265eV) as shown in Fig 10a compared to that of the bulk ZnO film (3.29 eV),[68] which is in good agreement with the absorption measurements.

The peak intensity map (Fig 10b) and FWHM map (Fig 10c) demonstrate that the NBE peak of the NRs has a high intensity and a narrow width. In addition, no defect band is observed from RT-CL spectrum of a single NR (Fig. S4, ESI,†), demonstrating a high crystalline quality of the NRs., which
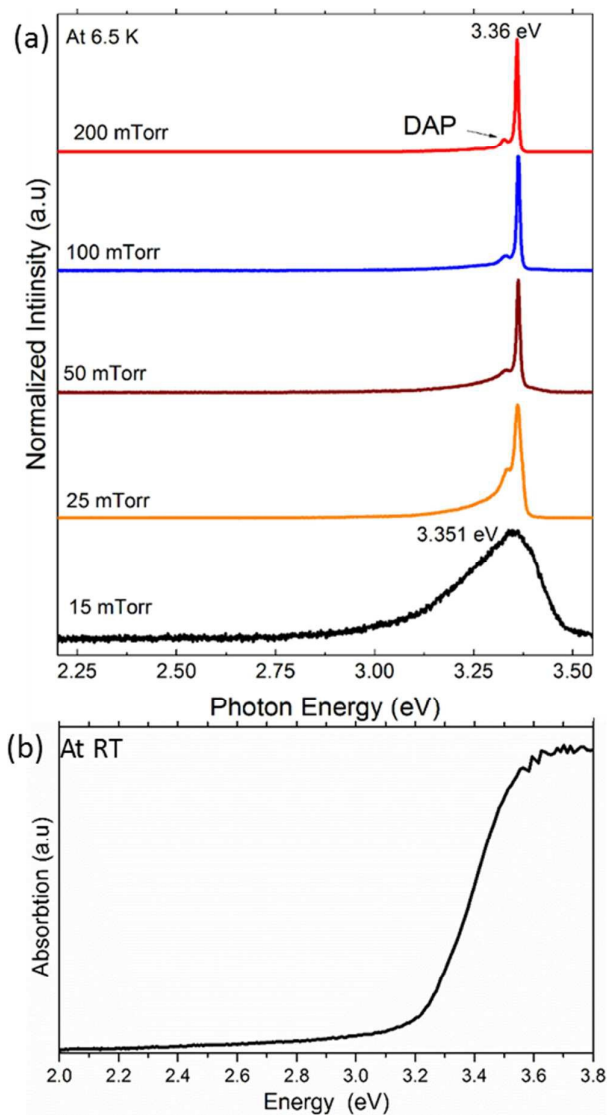


Fig 9. (a) PL spectra of ZnO NRs deposited at $P(O_2)$ =15, 25, 50, 100 and 200 mTorr, (b) Absorption spectrum of ZnO NRs deposited at P(O2) =200 mTorr.

agrees with low temperature PL.

The advantage of this method is that it allows for deposition of the metal oxide onto a transparent substrate at a suitable temperature based on the surface energy law using RE nanolyer. Although a pre-fabricated seed layer was not used in this work, the resulting NRs were well controlled with good structural, electrical, and optical properties. Therefore, the high electrical and optical quality of These NRS confirm their potential for optoelectronic, photovoltaic and electronic devices.

## Conclusions

To the best of our knowledge, we have developed a novel one-step method that demonstrates significant improvements in the formation of homogeneous, ideal, well-ordered vertical

RSC Advances Accepted Manuscript
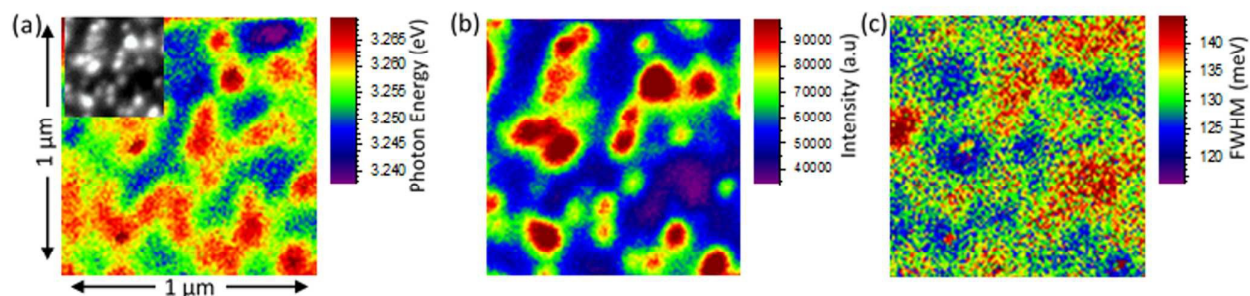
Fig 10. RT-CL hyperspectral maps (1×1 $\mu$m) of NRs deposited at 50 mTorr. CL map of (a) the spectral maximum energy (the top left inset presents the corresponding SE images), (b) the NBE emission intensity and (c) the FWHM of the NBE peak.

NRs on a transparent, conductive, uniform nanolayer without using a pre-fabricated template. The strain relaxation mechanism shows that the dislocation distribution varies as the thickness of the ZnO wetting layer increases and dislocation density declines rapidly in the interface between the ZnO wetting layer and the NRs. This high optical and electrical quality NR structure shows improvement for a wide range of electronic and optoelectronic properties. The mobility observed in the ZnO NRs is comparable with previous reports. We confirm that the lattice-matched $a$-Al$_2$O$_3$ substrates and the Gd dopants assist in the *in situ* formation of a uniform Gd interfacial nanolayer, which controls the homogeneity of the ZnO NR structure. This method can be generalized for different oxide materials and for optoelectronic and electronic devices.

## Acknowledgements

## References

1.   U. Ozgur, Y. I. Alivov, C. Liu, A. Teke, M. A. Reshchikov, S. Dogan, V. Avrutin, S. J. Cho and H. Morkoc, *Journal of Applied Physics*, 2005, **98**,041301.
2.   J. L. Gomez and O. Tigli, *Journal of Materials Science*, 2013, **48**, 612-624.
3.   M. Willander, O. Nur, Q. X. Zhao, L. L. Yang, M. Lorenz, B. Q. Cao, J. Z. Perez, C. Czekalla, G. Zimmermann, M. Grundmann, A. Bakin, A. Behrends, M. Al-Suleiman, A. El-Shaer, A. C. Mofor, B. Postels, A. Waag, N. Boukos, A. Travlos, H. S. Kwack, J. Guinard and D. L. Dang, *Nanotechnology*, 2009, **20**, 332001
4.   M. Laurenti, G. Canavese, A. Sacco, M. Fontana, K. Bejtka, M. Castellino, C. F. Pirri and V. Cauda, *Advanced Materials*, 2015, **27**, 4218-4223.
5.   J. Schrier, D. O. Demchenko and L.-W. Wang, *Nano Letters*, 2007, **7**, 2377-2382.
6.   X.-Y. Chen, T. Ling and X.-W. Du, *Nanoscale*, 2012, **4**, 5602-5607.
7.   X. D. Wang, J. Zhou, C. S. Lao, J. H. Song, N. S. Xu and Z. L. Wang, *Advanced Materials*, 2007, **19**, 1627-1631.
8.   K. K. Naik, R. Khare, D. Chakravarty, M. A. More, R. Thapa, D. J. Late and C. S. Rout, *Applied Physics Letters*, 2014, **105**, 233101
9.   I. Gonzalez-Valls and M. Lira-Cantu, *Energy & Environmental Science*, 2009, **2**, 19-34.
10.  C.-H. M. Chuang, P. R. Brown, V. Bulovic and M. G. Bawendi, *Nature Materials*, 2014, **13**, 796-801.
11.  Q. Hu, Y. Li, F. Huang, Z. Zhang, K. Ding, M. Wei and Z. Lin, *Scientific Reports*, 2015, **5**, 11499.
12.  H. Chen, L. Zhu, H. Liu and W. Li, *Nanotechnology*, 2012, **23**, 075402.
13.  Q. Wan, Q. H. Li, Y. J. Chen, T. H. Wang, X. L. He, J. P. Li and C. L. Lin, *Applied Physics Letters*, 2004, **84**, 3654-3656.
14.  X. Xiao, L. Yuan, J. Zhong, T. Ding, Y. Liu, Z. Cai, Y. Rong, H. Han, J. Zhou and Z. L. Wang, *Advanced Materials*, 2011, **23**, 5440-5444.
15.  M. R. Alenezi, S. J. Henley, N. G. Emerson and S. R. P. Silva, *Nanoscale*, 2014, **6**, 235-247.
16.  H. Chen, Z. Wei, K. Yan, Y. Bai, Z. Zhu, T. Zhang and S. Yang, *Small*, 2014, **10**, 4760-4769.
17.  Z. L. Wang and J. H. Song, *Science*, 2006, **312**, 242-246.
18.  M. K. Gupta, J.-H. Lee, K. Y. Lee and S.-W. Kim, *Acs Nano*, 2013, **7**, 8932-8939.
19.  G. Nagaraju, Y. H. Ko and J. S. Yu, *Materials Chemistry and Physics*, 2015, **149**, 393-399.
20.  S. Wang, C. Song, K. Cheng, S. Dai, Y. Zhang and Z. Du, *Nanoscale Research Letters*, 2012, **7**, 246.
21.  T. Ngo-Duc, K. Singh, M. Meyyappan and M. M. Oye, *Nanotechnology*, 2012, **23**, 194015-194015.
22.  R. Zhu, W. G. Zhang, C. Li and R. S. Yang, *Nano Letters*, 2013, **13**, 5171-5176.
23.  J. Joo, B. Y. Chow, M. Prakash, E. S. Boyden and J. M. Jacobson, *Nature Materials*, 2011, **10**, 596-601.
24.  D. Tsivion, M. Schvartzman, R. Popovitz-Biro, P. von Huth and E. Joselevich, *Science*, 2011, **333**, 1003-1007.
25.  S. S. Lin, J. I. Hong, J. H. Song, Y. Zhu, H. P. He, Z. Xu, Y. G. Wei, Y. Ding, R. L. Snyder and Z. L. Wang, *Nano Letters*, 2009, **9**, 3877-3882.

26. J. P. Kar, J.-H. Choi, S. N. Das, J. Xiong, M.-J. Lee, T. I. Lee and J.-M. Myoung, *Journal of Nanoscience and Nanotechnology*, 2011, **11**, 2185-2190.

27. C. V. Varanasi, K. D. Leedy, D. H. Tomich, G. Subramanyam and D. C. Look, *Nanotechnology*, 2009, **20**, 385706.

28. D. Yu, L. Hu, J. Li, H. Hu, H. Zhang, Z. Zhao and Q. Fu, *Materials Letters*, 2008, **62**, 4063-4065.

29. J.-I. Hong, J. Bae, Z. L. Wang and R. L. Snyder, *Nanotechnology*, 2009, **20**, 085609.

30. L. E. Greene, M. Law, D. H. Tan, M. Montano, J. Goldberger, G. Somorjai and P. D. Yang, *Nano Letters*, 2005, **5**, 1231-1236.

31. X. Wang, J. Song, J. Liu and Z. L. Wang, *Science*, 2007, **316**, 102-105.

32. T. Premkumar, Y. S. Zhou, Y. F. Lu and K. Baskar, *Acs Applied Materials & Interfaces*, 2010, **2**, 2863-2869.

33. R. Q. Guo, J. Nishimura, M. Matsumoto, D. Nakamura and T. Okada, *Applied Physics a-Materials Science & Processing*, 2008, **93**, 843-847.

34. A. Rahm, M. Lorenz, T. Nobis, G. Zimmermann, M. Grundmann, B. Fuhrmann and F. Syrowatka, *Applied Physics a-Materials Science & Processing*, 2007, **88**, 31-34.

35. M. Lorenz, E. M. Kaidashev, A. Rahm, T. Nobis, J. Lenzner, G. Wagner, D. Spemann, H. Hochmuth and M. Grundmann, *Applied Physics Letters*, 2005, **86**, 143113.

36. J. M. Zavada, N. Nepal, J. Y. Lin, H. X. Jiang, E. Brown, U. Hommerich, J. Hite, G. T. Thaler, C. R. Abernathy, S. J. Pearton and R. Gwilliam, *Applied Physics Letters*, 2006, **89**, 152107.

37. P. Fons, K. Iwata, A. Yamada, K. Matsubara, S. Niki, K. Nakahara, T. Tanabe and H. Takasu, *Applied Physics Letters*, 2000, **77**, 1801-1803.

38. M. Subramanian, P. Thakur, M. Tanemura, T. Hihara, V. Ganesan, T. Soga, K. H. Chae, R. Jayavel and T. Jimbo, *Journal of Applied Physics*, 2010, **108**, 053904.

39. Q. Li, K. Gao, Z. Hu, W. Yu, N. Xu, J. Sun and J. Wu, *Journal of Physical Chemistry C*, 2012, **116**, 2330-2335.

40. Y. Sun, G. M. Fuge and M. N. R. Ashfold, *Chemical Physics Letters*, 2004, **396**, 21-26.

41. S. S. Kim and B. T. Lee, *Thin Solid Films*, 2004, 446, 307-312.

42. M. Yan, H. T. Zhang, E. J. Widjaja and R. P. H. Chang, *Journal of Applied Physics*, 2003, **94**, 5240-5246.

43. E. Uccelli, J. Arbiol, C. Magen, P. Krogstrup, E. Russo-Averchi, M. Heiss, G. Mugny, F. Morier-Genoud, J. Nygard, J. R. Morante and A. F. I. Morral, *Nano Letters*, 2011, **11**, 3827-3832.

44. H. Chen, J. Luo, T. Zeng, L. Jiang, Y. Sun, Z. Jiao, Y. Jin and X. Sun, *New Journal of Chemistry*, 2014, **38**, 3907-3916.

45. R. L. Penn and J. F. Banfield, *Science*, 1998, **281**, 969-971.

46. G. M. Dalpian and J. R. Chelikowsky, *Physical Review Letters*, 2006, **96**, 226802.

47. L. Pyziak, W. Obermayr, K. Zembrowska and M. Kuzma, *Semiconductor Physics Quantum Electronics & Optoelectronics*, 2003, **6**, 183-188.

48. Z. Y. Zhang and M. G. Lagally, *Science*, 1997, 276, 377-383.

49. A. P. Payne, W. D. Nix, B. M. Lairson and B. M. Clemens, *Physical Review B*, 1993, **47**, 13730-13736.

50. G. Cao, *NANOSTRUCTURES & NANOMATERIALS (Synthesis, properties, & application)*, Imperial college press, London, 2004.

51. J. H. Choi, D. Y. Kim, B. J. Hockey, S. M. Wiederhorn, J. E. Blendell and C. A. Handwerker, *Journal of the American Ceramic Society*, 2002, **85**, 1841-1844.

52. M. Kawakami, A. B. Hartanto, Y. Nakata and T. Okada, *Japanese Journal of Applied Physics Part 2-Letters*, 2003, **42**, L33-L35.

53. B. Sun and H. Sirringhaus, *Nano Letters*, 2005, **5**, 2408-2413.

54. W. Liang, B. D. Yuhas and P. Yang, *Nano Letters*, 2009, **9**, 892-896.

55. N. A. Jayah, H. Yahaya, M. R. Mahmood, T. Terasako, K. Yasui and A. M. Hashim, *Nanoscale Research Letters*, 2015, **10**, 7.

56. G. Kresse and J. Hafner, *Physical Review B*, 1993, **47**, 558-561.

57. G. Kresse and J. Furthmuller, *Physical Review B*, 1996, **54**, 11169-11186.

58. J. P. Perdew, K. Burke and M. Ernzerhof, *Physical Review Letters*, 1996, **77**, 3865-3868.

59. H. Shi, P. Zhang, S.-S. Li and J.-B. Xia, *Journal of Applied Physics*, 2009, **106**, 023910.

60. Y. Li, R. Deng, W. Lin, Y. Tian, H. Peng, J. Yi, B. Yao and T. Wu, *Physical Review B*, 2013, **87**, 155151.

61. G. M. Dalpian and S. H. Wei, *Physical Review B*, 2005, 72.

62. S. A. Aravindh, U. Schwingenschloegl and I. S. Roqan, *Journal of Applied Physics*, 2014, **116**, 233906.

63. S. Venkatesh, J. B. Franklin, M. P. Ryan, J. S. Lee, H. Ohldag, M. A. McLachlan, N. M. Alford and I. S. Roqan, *Journal of Applied Physics*, 2015, **117**, 013913

64. B. P. Zhang, N. T. Binh, Y. Segawa, K. Wakatsuki and N. Usami, *Applied Physics Letters*, 2003, **83**, 1635-1637.

65. A. Janotti and C. G. Van de Walle, *Reports on Progress in Physics*, 2009, **72**, 126501.

66. A. Cremades, L. Gorgens, O. Ambacher, M. Stutzmann and F. Scholz, *Physical Review B*, 2000, **61**, 2812-2818.

67. P. R. Edwards, L. K. Jagadamma, J. Bruckbauer, C. Liu, P. Shields, D. Allsopp, T. Wang and R. W. Martin, *Microscopy and Microanalysis*, 2012, **18**, 1212-1219.

68. Y. F. Chen, D. M. Bagnall, H. J. Koh, K. T. Park, K. Hiraga, Z. Q. Zhu and T. Yao, *Journal of Applied Physics*, 1998, **84**, 3912-3918.

# Homogeneous vertical ZnO nanorod arrays with high conductivity on an *in situ* Gd nanolayer

*Tahani H Flemban, S. Venkatesh, S. Assa Aravindh, Iman S Roqan\**

We demonstrate a novel, one-step, catalyst-free method for the production of size-controlled vertical highly conductive ZnO NR arrays with highly desirable characteristics by pulsed laser deposition using a Gd-doped ZnO target. Our study shows that an *in situ* transparent and conductive Gd nanolayer (with a uniform thickness of ~1 nm) at the interface between a lattice-matched (11-20) *a*-sapphire substrate and ZnO is formed during the deposition. This nanolayer significantly induces relaxation mechanism that controls the dislocation distribution along the growth direction; which consequently improves the formation of homogeneous vertically aligned ZnO NRs. We demonstrate that both the lattice orientation of the substrate and the Gd characteristics are important in enhancing the NR synthesis, and we report precise control of the NR density by changing the oxygen partial pressure. We show that these NRs possess high optical and electrical quality, with a mobility of 177 cm$^2$ (V.s)$^{-1}$, which is comparable to the best-reported mobility of ZnO NRs. Therefore, this new and simple method has significant potential for improving the performance of materials used in a wide range of electronic and optoelectronic applications.